International Journal of Engineering Applied Sciences and Technology, 2020
Vol. 5, Issue 1, ISSN No. 2455-2143, Pages 139-144
Published Online May 2020 in IJEAST (http://www.ijeast.com)

DETERMINATION OF THE MECHANICAL PROPERTIES OF TERNARY THIN FILM MEASURED BY NANO INDENTATION

Obasi, B. Ibe
Department of Physics/Electronics
Federal Polytechnic, Nekede, Owerri, Nigeria

Eze, Joseph. O.
Department of Physics/Electronics
Federal Polytechnic, Nekede, Owerri, Nigeria

Abstract - **The aim of this work was to determine the hardness and Young's modulus from data obtained from a nanoindenter that could accomplish detailed Nano-indentations in addition to high-resolution surface imaging. The penetration hardness was determined from the load-penetration depth curve acquired from this instrument, and the effective hardness and Young's modulus were computed from the gradient of the unloading curve. In addition, these methods were applied to measure the mechanical properties of ternary thin films of CuFeS and ZnFeS with varying concentrations of Cu and Zn ions deposited on glass substrate by the spray pyrolysis method. The penetration hardness on the films were computed to be ranging from 195.41 to 842.85MPa and 481.9 to 606.8MPa for the CuFeS and ZnFeS thin films respectively, with contact stiffness ranging from 31.5 to 33.5μN/nm and 16.3 to 28.1μN/nm in that order. The correspondingly effective elastic modulus were 19.49 to 60.88 and 22.41 to 30.63.**

Keywords - **Spray pyrolysis, Copper iron sulphide, Nano indentation, Contact stiffness, Loading-unloading curve**

I. INTRODUCTION

Abrasion and corrosion resistance in hard films materials deposited by chemical and physical deposition technique are being used in recent times. Hiromi et al. (2001); Vargas et al. (2019) and Bull (2019) reported that mechanical properties of films such as penetration hardness, contact stiffness and Young's modulus has become increasingly necessary to measure and evaluate the quality of these thin films. Thin film measurements require the use of very small indentations therefore; micro-Vickers hardness testers with a minimum load of 9.8mN are unsuitable and too heavy to apply on these films for determining their hardness. Nano-indentation hardness testers also referred to as Nanoindenters, has been established and has become the standard technique used for Nano mechanical characterization of materials. The nanoindentation test is performed by applying and removing a load to a sample in a highly controlled manner with a geometrically well-defined probe. During the nanoindentation process, a force is applied by the transducer and the probe displacement is continuously measured to produce a traditional force versus displacement curve. The resulting force-displacement curve serves as the mechanical characteristic of the material, from which quantitative nanoscale material properties can be determined. Oliver and Pharr (1992), El Khakani (2004) and Obasi et al. (2016) emphasized the common use of Nanoindenters for the determination of a sample's hardness and Young's modulus.

Our study, therefore, presents a technique for deducting the elastic displacement from the load-penetration curves to obtain the hardness. Doener and Nix (1982) described the method of connecting the elastic displacements to the Young's modulus of the sample, this method is reviewed is equally revisited. In this paper, we will establish the technique for determining the hardness, stiffness and Young's modulus of the thin film material from the load-penetration curve obtained from the nanoindenter. The technique will be applied to the ternary thin films of copper iron sulphide and zinc iron sulphide deposited on glass substrate by the spray pyrolysis method to real their mechanical properties.

II. METHODS AND MATERIALS

A. The Nanoindentation Test

The nanoindentation test was conducted with a commercially available nanoindenter, the Triboscope Testing System from Hysitron Inc. Hysitron measures the force and displacement of the nanoindentation probe with a unique patented three-plate capacitive transducer design. This transducer design provides an unsurpassed noise floor and ultra-low working force which is complemented in a study by Faisal, et al. (2014). The displacement resolutions and force of the nanoindenter are < 0.2nm and < 1nN, respectively. Integrated into a scanning probe microscope (SPM), this system can perform both precise Nano indents and high resolution surface imaging with a repulsive force of 1mN, which was collaborated by Lisunova et al. (2011). With some indentations, surface imaging was immediately achieved after the indentations had been formed. In this study, the load applied by the nanoindenter was very light, usually from 100 to 3000mN. The typical drift rate and testing rate was < 0.9nm/s and 50mN/s. The typical force outline was the trapezium, and the load was held at the maximum load for 10s. The indenter was a triangular pyramid-shaped diamond with an edge angle of $\theta = 115°$ (Berkovich indenter). The nanoindentation test was repeated five times under same conditions. The typical load-penetration depth curve obtained from the nanoindenter is shown in Fig. 1. Doener and Nix, (1982) reported the coordinate (h_c) as the intersection point of a straight line obtained from the removal

International Journal of Engineering Applied Sciences and Technology, 2020
Vol. 5, Issue 1, ISSN No. 2455-2143, Pages 139-144
Published Online May 2020 in IJEAST (http://www.ijeast.com)

data of 1/3 of the maximum load by the method of least squares with abscissa. The coordinate (h_f) shows the position where the indenter becomes detached from the specimen surface. The coordinate (h_{max}) shows the position at which the penetration depth of the indenter into the specimen has reached its maximum value.

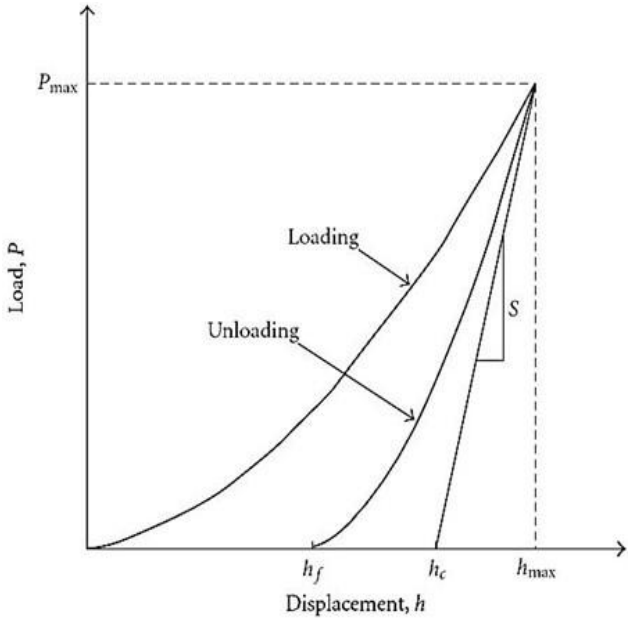

Fig. 1. Typical load-displacement curve.

B. Measurements of Young's modulus and hardness

Figure 1 represents a schematic of a typical data set obtained with a Berkovich indenter, where the load is designated as P, the displacement is designated as h. The deformation during loading is assumed to be both elastic and plastic in nature as the permanent hardness impression forms. During, unloading it is assumed that only the elastic displacements are recovered.

The three quantities measured from the load-displacement curve are the maximum load P_{max}, the maximum displacement h_{max} and the elastic unloading stiffness, S = dp/dh, defined as the slope of the upper portion of the unloading curve during the initial stages of unloading (also called contact stiffness). Another useful quantity is the permanent depth of penetration after the indenter is fully unloaded designated as h_f (final depth).

Oliver and Pharr (1992) showed from experiments that the unloading curves are distinctly curved and usually well approximated by the power law relation:

$$P = \alpha(h - h_f)^m \quad (1)$$

where α and m are power law fitting constants.

Further literature from Oliver and Pharr (2004) described the Berkovich indenter modeled by a conical indenter as shown in Figure 2, with a half-included angle, ϕ, that gives the same depth-to-area relationship. This basic assumption is that the contact periphery sinks like model for indentation of a flat elastic half-space by rigid punches of simple geometry, with the limitation of not accounting for pile up of material at the contact periphery that occurs in some elastic-plastic materials.

Doemer & Nix (1986) equated h_s while neglecting pile-up, the amount of sink-in, as:

$$h_s = \epsilon \frac{P_{max}}{S} \quad (2)$$

where ∈ is constant depending on the indenter geometry.

Reynaud et al. (2000) and Aso et al. (2007) described useful values of ∈ = 0.77 for conical punch; ∈ = 0.75 for a paraboloid of revolution and ∈ = 1 for punch.

C. The penetration hardness -

The effective indenter shape ∈ can be determined using Snedden's method for determining the surface displacement at the contact perimeter for indentation with a rigid punch by the Eq. (3). Finite element studies showed that the effective indenter shape is well approximated by the power relation.

$$Z = Br^n \quad (3)$$

where B is a fitting constant and the exponent n varies in the range 2-6 depending on the material properties (Oliver and Pharr, 2004) in conjunction with Eq. (2) yields:

$$\epsilon = m\left[1 - \frac{2\,\Gamma\left(\frac{m}{2(m-1)}\right)}{\sqrt{\pi}\,\Gamma\left(\frac{1}{2(m-1)}\right)}(m-1)\right] \quad (4)$$

Note that the range of expected m is 1.2 to 1.6, and ∈ varies between 0.74 and 0.79 where Γ is the factorial function.

International Journal of Engineering Applied Sciences and Technology, 2020
Vol. 5, Issue 1, ISSN No. 2455-2143, Pages 139-144
Published Online May 2020 in IJEAST (http://www.ijeast.com)

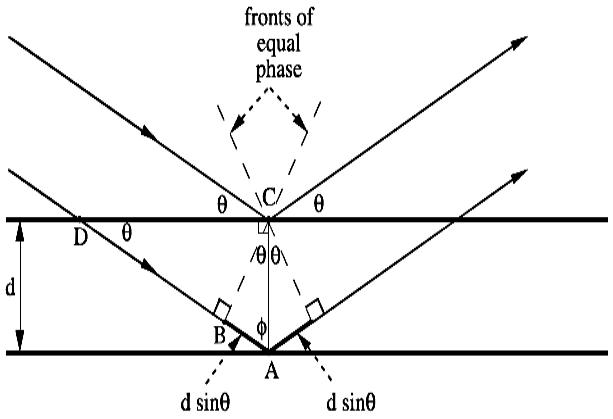

Fig. 2. Geometry for interference of a wave scattered from two planes separated by spacing, *d*.

Based on the observation that the unloading curves are best approximated by an indenter that behaves like a paraboloid is the standard for this analysis from the geometry of Fig. 2 and using Eq. (2) it follows that the depth between the indenter and the specimen is:

$$h_c = h_{max} - h_s \tag{5}$$

hence

$$h_s = h_{max} - \epsilon \frac{P_{max}}{S} \tag{6}$$

Let F(d) be cross sectional area of the indenter at a distance d back from its tip, the contact area A is then:

$$A = F(h_c) \tag{7}$$

The hardness of the samples can then be estimated from

$$H = \frac{P_{max}}{A} \tag{8}$$

Measurement of the elastic modulus follows from the relation of contact area and the unloading stiffness stated in Equation (9) reported by Oliver et al. (1992); Schwiedrzik and Zysset, (2015):

$$S = \beta \frac{2}{\sqrt{\pi}} E_{eff} \sqrt{A} = C_A E_{eff} \sqrt{A} \tag{9}$$

where $C_A = \beta \frac{2}{\sqrt{\pi}}$ and $E_{eff.}$

Hashin, (2013) and Wendt, (2013) defined the effective elastic modulus by:

$$\frac{1}{E_{eff}} = \frac{1 - v^2}{E} = \frac{1 - v_i^2}{E_i} \tag{10}$$

where E is Young's modulus, v is Poisson's ratio, E_i and v_i elastic constants. Fukuhara & Yamauchi (1993) described how the Young's modulus and Poisson's ratio can be calculated using Eq. (11) and (12).

$$E = 3\rho V_s^2 \frac{V_h^2 - \left(\frac{4}{3}\right) V_s^2}{V_h^2 - V_s^2} \tag{11}$$

$$v = ½ \left\{ 1 - \frac{1}{\left(\frac{v_h}{v_s}\right)^2 - 1} \right\} \tag{12}$$

where V_h and V_s are the velocity of the longitudinal and transverse sound wave measured by the ultrasonic pulse method, and P is the density of the specimen.

Note that Eq. (9) is a general relation that is not specific to any simple geometry, and it is unaffected by pile-up and sink-in. The dimensionless parameter β (correction factor) plays a very important role when desiring accurate property measurement. B = 1 for the case of small deformation of an elastic material by rigid axisymmetric punch of smooth profile. B = 1.012 for a square-based indenter, β = 1.034 for a triangular punch and β = 1.058 for the flat-ended triangular punch (Kan et al., 2013). In this work, we assumed β is 1.

III. RESULTS AND DISCUSSION

The nanoindentation test was carried out for all the samples using the Berkovich indenter to determine the constant (C_A). The Young modulus and the Poisson's ratio of the diamond used are E = 1210GPa and v = 0.20 respectively. In Figure 3, we present the load-unloading data obtained in nanoindentation tests for all samples of CuFeS and ZnFeS. The slope of the unloading curve is calculated from the differential forms of Eq. (1) with respect to h.

$$\frac{d}{dh} P = \alpha\, m \left(h - h_f\right)^{m-1} \tag{13}$$

where α, m and h_f are constants.

From literature the constant (C_A) increases as the load decreases, also C_A increases as the penetration depth (h_{max}) decreases. The result of the relationship between C_A, load and penetration can be approximated by Eq. (14)

$$C_A = 0.91 + \frac{22.7}{h_{max} - 10.3} \tag{14}$$

The constant C_A is calculated from Eq. (14) in this work. The mechanical properties of the substance using very heavy loads influence the measurement of the hardness and Young's modulus of the thin film. Investigation reported that in determining the effect of the load, varying loads were used to

International Journal of Engineering Applied Sciences and Technology, 2020
Vol. 5, Issue 1, ISSN No. 2455-2143, Pages 139-144
Published Online May 2020 in IJEAST (http://www.ijeast.com)

measure the effective young's modulus and contact stiffness of the film. Ishikawa et al., (2001); Musil et al, (2002); Xiang et al. (2017) work showed that the effective young's modulus decreases with increase in the penetration depth (h_{max}).

This is in agreement with the results obtained from calculating the mechanical properties using computer programme (Triboscan). Table 1 represents the calculated values from our model and the Triboscan results for investigated mechanical properties of X1 and Y1. The hardness of the films was 481.9 and 544.4MPa for CuFeS and ZnFeS respectively, with a load of 400µN. The ZnFeS film seems to be much harder than the CuFeS film. The stiffness of the films was 16.3 and 21.5µN/nm for CuFeS and ZnFeS respectively. The effective elastic modulus was 22.4 and 24.5GPa in that order.

Table 1. Comparison of indentation result between our models with a computer generated result (Triboscan).

Sample	S (µN/nm)		H (MPa)		E_{eff} (GPa)	
	A	B	A	B	A	B
CuFeS	31.5	31.7	195.41	197.51	19.7	19.49
ZnFeS	16.3	15.9	481.9	480.3	22.4	22.6

* A = our model; B = compute generated; S = stiffness H = hardness, E_e = effective elastic modulus,

The average of all the calculated Nano-indentation parameters for CuFeS of different Cu concentrations (X1, X2 and X3) of interest in this work. Figures 3-5 shows the loading and unloading curves for CuFeS sample. An excursion can be observed (shaded portion) on the loading curves. Each of them corresponds to an event of crack propagation or a fracture. The effective penetration (heff) is 215nm under a load of 400µN for X1 thin film. Equally, the X2 sample computed values the effective penetration (heff) was 164nm, under a load of 400µN for X1 thin films. The heff, for X3 was 59nm, under a load of 200µN. The hardness test for ZnFeS thin film of varying Zn ion concentration are shown in Figures 6-8, the figures showed that the maximum displacement occurred at 92.5nm under a load of 200µN for ZnFeS (Y1) sample. The effective penetration (h_{eff}) of Y2 was 86nm at a maximum displacement of 115.36nm, under a load of 400µN. While for ZnFeS (Y3) thin film the h_{eff}, displacement and force were 118.86nm and 400 µN in that order. Table 2 represents the summary of all calculated parameters of the samples.

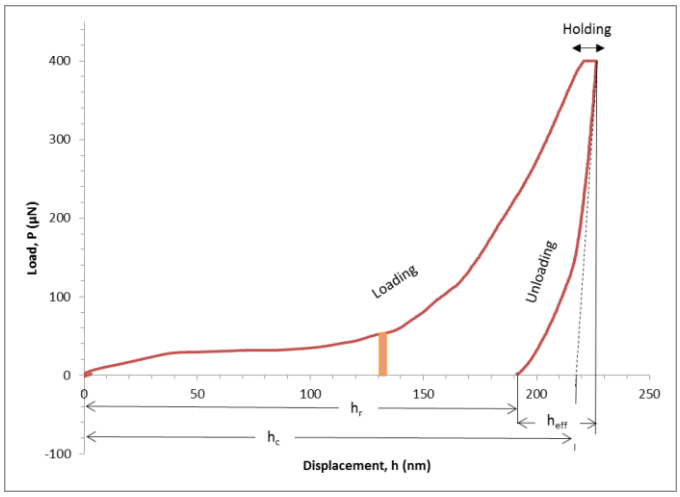

Fig. 3. Loading-unloading curves of CuFeS (X1).

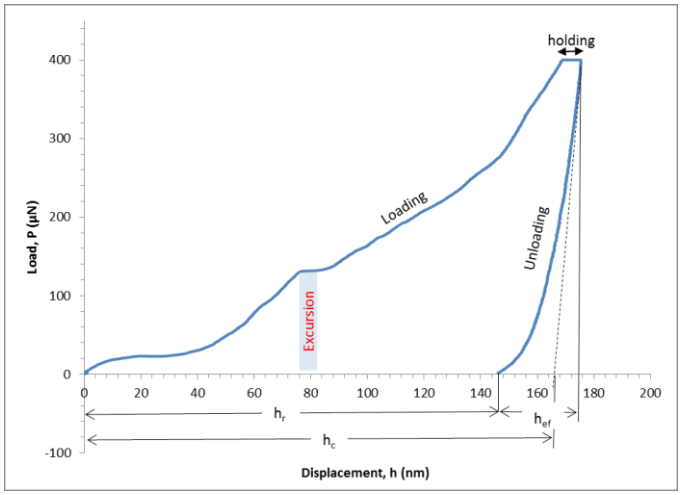

Fig. 4. Loading-unloading curves of CuFeS (X2).

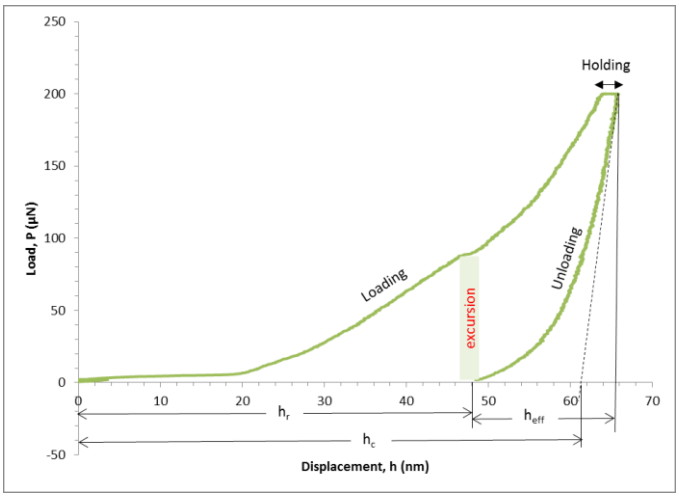

International Journal of Engineering Applied Sciences and Technology, 2020
Vol. 5, Issue 1, ISSN No. 2455-2143, Pages 139-144
Published Online May 2020 in IJEAST (http://www.ijeast.com)

Fig. 5. Loading-unloading curves of CuFeS (X3).

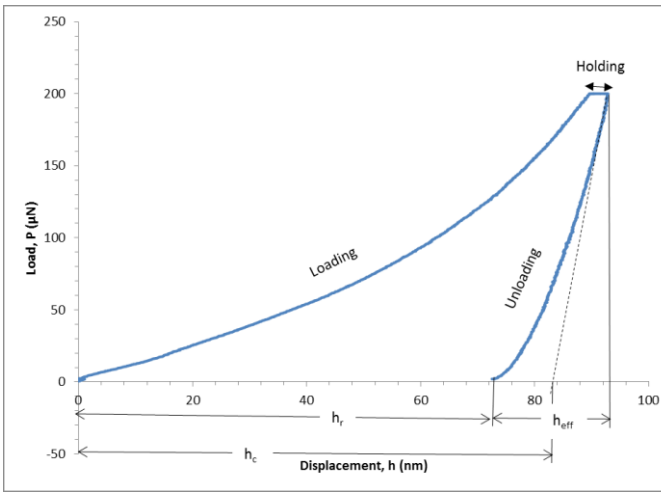

Fig. 6. Loading-unloading curves of ZnFeS (Y1)

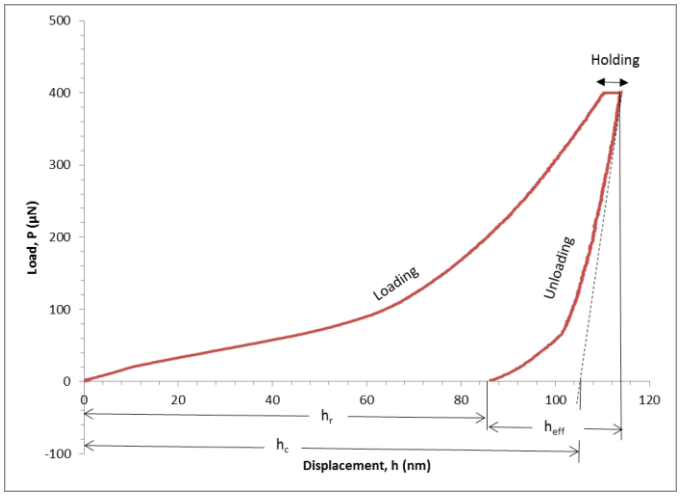

Fig. 7. Loading-unloading curves of ZnFeS (Y2).

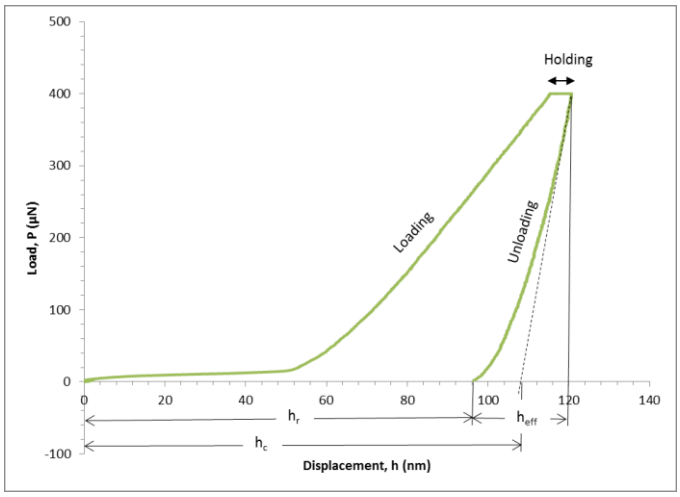

Fig. 8. Loading-unloading curves of ZnFeS (Y3).

Table 2. Calculated values of CuFeS and ZnFeS samples

ID	h_c (nm)	h_{max} (nm)	A (nm^2) x10^6	S (μN /nm)	H (MPa)	E_e (MPa)
X1	217.8	227.3	2.05	31.5	195.41	19.49
X2	166.3	175.7	1.31	31.9	305.94	24.72
X3	61.4	65.9	2.37	33.5	842.85	60.88
Y1	83.9	93.1	0.41	16.3	481.9	22.41
Y2	102.7	119.3	0.53	21.5	544.41	24.49
Y3	110.2	120.9	0.66	28.1	606.8	30.63

* h_c = contact depth, h_{max} = max, depth A = contact area, S = stiffness, H = hardness, E_e = effective elastic modulus.

IV. CONCLUSION

The penetration hardness is dependent on the load. To determine the penetration hardness and effective young modulus accurately, the load should be set so that the ratio of the penetration depth to the film thickness is less than 0.1. The constant C_A is dependent on the penetration depth and increases as the penetration depth decreases (i.e. h_{max} α $1/C_A$) the penetration hardness for the films ranged from 195.41 to 842.85MPa and 481.9 to 606.8MPa for the CuFeS and ZnFeS films.

V. REFERENCE

[1] Aso, O., Eguiazábal, J.I. and Nazábal, J. (2007). The influence of surface modification on the structure and properties of a nanosilica filled thermoplastic elastomer. Composites science and technology, 67(13), (pp. 2854-2863).

[2] Bull, S.J. (2019). Microstructure and indentation response of TiN coatings: The effect of measurement method. Thin Solid Films, 688, (pp.137452).

[3] Doerner, M.F. and Nix, W.D. (1986). A method for interpreting the data from depth sensing indentation

instruments, Journal of Materials Research 1(4): (pp. 601 – 609).

[4] El Khakani, M. A., Chaker, M., Jean, A., Boily, S., Kieffer, J. C., O'hern, M. E., and Rousseaux, F. (1994). Hardness and Young's modulus of amorphous a-SiC thin films determined by nanoindentation and bulge tests, Journal of materials research, 9(1), (pp. 96-103).

[5] Faisal, N.H., Ahmed, R., Goel, S. and Fu, Y.Q. (2014). Influence of test methodology and probe geometry on nanoscale fatigue failure of diamond-like carbon film, Surface and coatings technology, 242, (pp.42-53).

[6] Hashin, Z., & Herakovich, C.T. (Eds.). (2013). Mechanics of composite materials: recent advances. Elsevier.

[7] Ishikawa, H.; Fudetani, S.; Hirohashi, M. (2001). Mechanical properties of thin films measured by nanoindenters; Applied surface science, 178(1), (pp. 56-62).

[8] Kan, Q., Yan, W., Kang, G., and Sun, Q. (2013). Oliver–Pharr indentation method in determining elastic moduli of shape memory alloys—a phase transformable material; Journal of the Mechanics and Physics of Solids, 61(10), (pp. 2015-2033).

[9] Lisunova, M., Drachuk, I., Shchepelina, O., Anderson, K., and Tsukruk, V. (2011). Direct probing of micromechanical properties of hydrogen-bonded layer-by-layer microcapsule shells with different chemical compositions; Langmuir, 27(17), (pp. 11157-11165).

[10] Musil, J., Kunc, F., Zeman, H., & Polakova, H. (2002). Relationships between hardness, Young's modulus and elastic recovery in hard nanocomposite coatings, Surface and Coatings Technology, 154(2-3), (pp. 304-313).

[11] Obasi, B.I., Onyewenjo, S. and Omenikolo, A., (2016). Effects of grapheme materials on microorganisms and cells of living systems, ASUPNEK Journal of Empirical Research, 1(3), (pp. 6-12).

[12] Oliver, W.C., and Pharr, G.M. (1992). An improved technique for determining hardness and elastic modulus using load and displacement sensing indentation experiments, Journal of materials research, 7(06), (pp. 1564-1583).

[13] Oliver, W.C., and Pharr, G.M. (2004). Measurement of hardness and elastic modulus by instrumented indentation: Advances in understanding and refinements to methodology; Journal of materials research, 19(01), (pp. 3-20).

[14] Pharr, G.M., Oliver, W.C., & Brotzen, F. R. (1992). On the generality of the relationship among contact stiffness, contact area, and elastic modulus during indentation, Journal of materials research, 7(3), (pp. 613-617).

[15] Reynaud, C., Sommer, F., Quet, C., El Bounia, N., and Duc, T.M. (2000). Quantitative determination of Young's modulus on a biphase polymer system using atomic force microscopy. Surface and Interface Analysis: An International Journal devoted to the development and application of techniques for the analysis of surfaces, interfaces and thin films, 30(1), (pp. 185-189).

[16] Schwiedrzik, J.J., & Zysset, P.K. (2015). Quantitative analysis of imprint shape and its relation to mechanical properties measured by microindentation in bone; Journal of biomechanics, 48(2), (pp. 210-216).

[17] Vargas, A.L.M., Blando, E. and Hübler, R. (2019). Elasto–Plastic materials behavior evaluation according to different models applied in indentation hardness tests; Measurement, 139, (pp.134-139).

[18] Wendt, F.W., Liebowitz, H., & Perrone, N. (Eds.). (2013). Mechanics of Composite Materials, Proceedings of the Fifth Symposium on Naval Structural Mechanics; Elsevier.

[19] Xiang, Z., Zhang, L., Li, Y., Yuan, T., Zhang, W., & Sun, J. (2017). Reduced graphene oxide-reinforced polymeric films with excellent mechanical robustness and rapid and highly efficient healing properties, ACS nano, 11(7), (pp. 7134-7141).